Supporting Information

Electron-Triggered Metamorphism in Palladium-Driven Self-Assembled Architectures

Christophe Kahlfuss,† Shagor Chowdhury,† Adérito Fins Carreira,† Raymond Grüber,† Elise Dumont,†,§ Denis Frath,† Floris Chevallier,† Eric-Saint-Aman‡ and Christophe Bucher†**

† Univ Lyon, Ens de Lyon, CNRS UMR 5182, Université Claude Bernard Lyon 1, Laboratoire de Chimie, F69342 Lyon, France.

‡ Univ. Grenoble Alpes, CNRS, Département de Chimie Moléculaire, F38000 Grenoble, France.

§ Institut Universitaire de France, 5 rue Descartes, 75005 Paris.

Contents

1. General Synthesis

Solvents and Reagents

All reagents were obtained commercially unless otherwise noted. All reactions were performed in oven-dried glassware (Schlenk flasks) under an argon atmosphere. All solvents were dried and distilled by standard procedures. Flash column chromatography separations were achieved on silica gel (VWR 40-63 μm). *Cis*-(ethylenediamine)dinitratopalladium(II), *trans*-bis(acetonitrile)dichloro-palladium(II) and $\mathbf{4}^{2+}$ have been prepared following procedures described in the literature.[S1-S3]

Apparatus and Spectroscopic Characterizations

^{1}H-NMR and ^{13}C-NMR spectra were recorded at room temperature on a Bruker Avance 500 MHz spectrometer. ^{1}H chemical shifts were referenced to residual solvent peaks. Coupling constants values (J) are given in hertz and chemical shifts (δ) in ppm. The abbreviations used are: s = singlet, d = doublet, t = triplet, m = multiplet and br = broad.

UV/Vis spectra were recorded on a MCS 500 or MCS 601 UV-NIR Zeiss spectrophotometer using all-quartz immersion probes (Hellma Inc.). Mass spectrometry measurements were carried out at the "Centre commun de spectrométrie de masse – Lyon 1" mass spectrometry facility with a MicrOTOFQ II(Bruker) using electrospray ionization (ESI). Elemental analyses (C, H and N) were carried out on a Perkin–Elmer 240 at the "Département de Chimie Moléculaire – Grenoble" microanalysis facility.

2. Electrochemical Studies

Solvents and Electrolytes

Acetonitrile (Acros Organics, extra-dry with molecular sieves, water < 0.005%), dimethylformamide (Sigma Aldrich, extra-dry with molecular sieves, water < 0.01%) were degassed using Freeze-Pump-Thaw procedure and were used for the spectroelectrochemical studies. The electrolyte tetra-*n*-butylammonium perchlorate (TBAP, Fluka puriss.) was purchased and used without further purification.

Apparatus and Spectroelectrochemical Characterization

Cyclic voltammetry (CV) and voltammetry with rotating disc electrodes (RDE) were recorded using a SP300 Bilogic potentiostat. The analytical studies were conducted under an argon atmosphere (glove box or argon stream) in a standard one–compartment, three–electrodes electrochemical cell. Tetra-*n*-butylammonium was used as supporting electrolytes (0.1 M). An automatic ohmic drop compensation procedure was systematically performed when using cyclic voltammetry. Vitreous carbon (Ø = 3 mm) working electrodes (CH Instruments) were polished with 1 mm diamond paste before each recording. Voltamperometry with a rotating disk electrode (RDE) was carried out with a radiometer (CTV101 radiometer analytical) equipment at a rotation rate of 500 rad min^{-1} using a glassy carbon RDE tip (Ø= 3 mm).

Spectroelectrochemical measurements were carried out at room temperature under an argon atmosphere (glove box or argon stream) in a standard one–compartment, three–electrodes electrochemical cell with a biologic SP300 potentiostat coupled to an MCS 500 or MCS 601 UV-NIR Zeiss spectrophotometer using 1 or 10 mm all–quartz Helmma immersion probes. Electrolyses were conducted at room temperature using platinum plates (10 cm^2) working electrodes and a large piece of carbon felt as a counter–electrode isolated from the electrolytic solution through an ionic bridge. $Ag/AgNO_3$ (CH Instruments, 10^{-2} M + TBAP 10^{-1} M in CH_3CN) was used as a reference electrode.

2. Experimental procedures and characterizations

2.1 Synthesis of **2**$(Cl)_2$

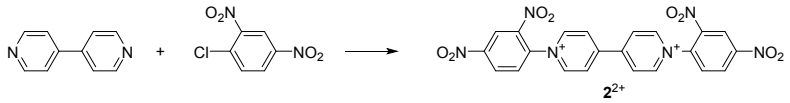

Compound $\mathbf{2}^{2+}$ was prepared from 4,4'-bipyridine and 2,4-dinitro-chlorobenzene in acetonitrile according to a literature[S4] procedure in 70% isolated yield. ^{1}H NMR (D_2O, 300 MHz): δ = 8.33 (d, 2H, *J* = 8.7 Hz), 8.95 (d, 4H, *J* = 6.3 Hz), 8.97 (dd, 2H, *J* = 2.1 and 8.7 Hz), 9.44 (d, 2H, *J* = 2.1 Hz), 9.50 ppm (d, 4H, *J* = 6.3 Hz). These values are consistent with those reported in the literature.[S4]

2.2 Synthesis of **3**

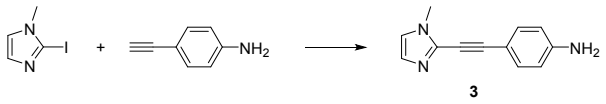

To a stirred, degassed solution of 4-ethynylaniline (117 mg, 1.0 mmol), 2-iodo-1-methyl-1*H*-imidazole [S5] (208 mg, 1.0 mmol), copper(I) iodide (9.5 mg, 5 mol %), in triethylamine (4 mL) and tetrahydrofuran (16 mL) was added bis(triphenylphosphine)palladium(II) dichloride (70 mg, 10 mol %). The reaction mixture was stirred for 18 h at 60 °C and subsequently concentrated under reduced pressure. Purification by flash chromatography on silica gel (ethyl acetate/cyclohexane: 1/1) gave **3** (172 mg, 87%) as a yellow solid. ^{1}H NMR ($CDCl_3$, 300 MHz): δ = 3.76 (s, 3H), 3.78 (br s, 2H), 6.63 (d, 2H, *J* = 8.4 Hz), 6.90 (s, 1H), 7.06 (s, 1H), 7.36 ppm (d, *J* = 8.4 Hz, 2H). ^{13}C NMR ($CDCl_3$, 100 MHz): δ = 33.7, 66.8, 84.9, 93.7, 111.1, 114.8 (2C), 121.4, 129.7, 133.3 (2C), 147.5 ppm. HRMS (ESI): calcd for $C_{12}H_{12}N_3$ $[M+H]^+$ 198.1031, found 198.1030.

2.3 Synthesis of **1**$(PF_6)_2$

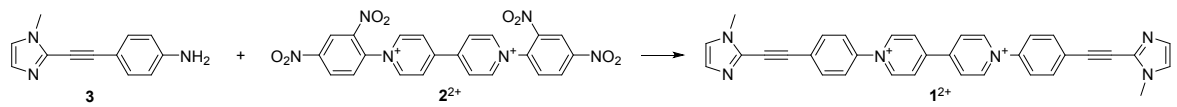

To a stirred solution of **2**$(PF_6)_2$ (78 mg, 0.1 mmol) in ethanol (10 mL) and acetonitrile (10 mL) was added **3** (43 mg, 0.22 mmol). The reaction mixture was stirred for 6 h at 80 °C and

subsequently concentrated under reduced pressure. Purification by flash chromatography on silica gel (acetonitrile/water/saturated aqueous potassium nitrate: 100/15/2.5) and anion exchange using an aqueous saturated KPF_6 solution, gave **1**$(PF_6)_2$ (31 mg, 38%) as an orange solid. ^{1}H NMR (DMSO-d_6, 400 MHz): δ = 3.84 (s, 6H), 7.08 (d, 2H, *J* = 0.9 Hz), 7.42 (d, 2H, *J* = 0.9 Hz), 8.07 (s, 8H), 9.10 (d, 4H, *J* = 7.0 Hz), 9.74 ppm (d, 4H, *J* = 7.0 Hz). ^{13}C NMR ($CDCl_3$, 100 MHz): δ = 32.2 (2C), 83.5, 90.7, 124.2, 126.1 (4 CH), 127.1, 128.4 (4 CH), 130.7, 132.1, 134.4 (4 CH), 143.0, 146.6 (4 CH), 151.4 ppm. HRMS (ESI): calcd for $C_{34}H_{26}N_6^{2+}$ $[M\text{-}2PF_6]^{2+}$ 259.1109, found 259.1112.

3. HRMS spectra

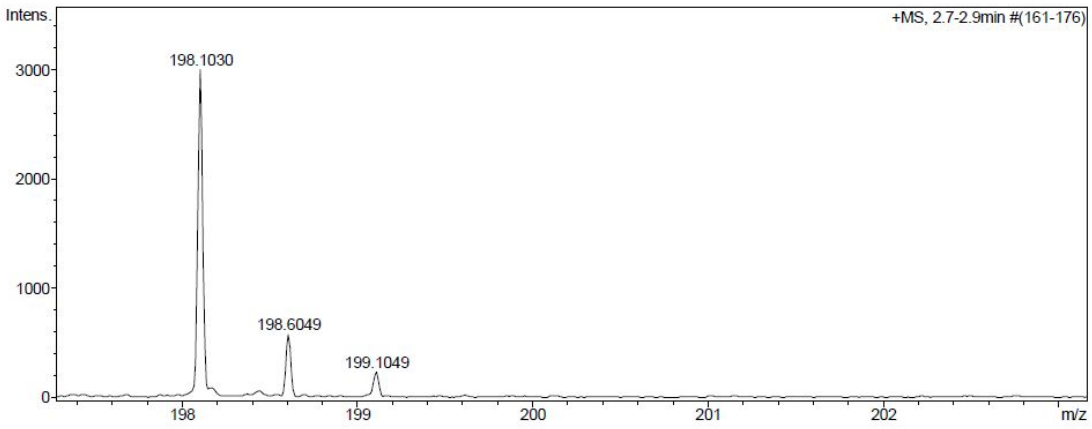

Figure S1. HRMS spectrum of **3** (calcd for $C_{12}H_{12}N_3$ $[M+H]^+$ 198.1031, found 198.1030)

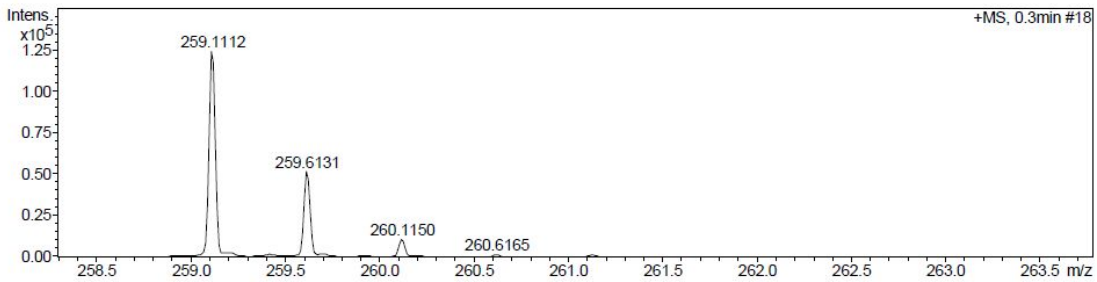

Figure S2. HRMS spectrum of **1**$^{2+}$ (calcd for $C_{34}H_{26}N_6^{2+}$ $[M\text{-}2PF_6]^{2+}$ 259.1109, found 259.1112

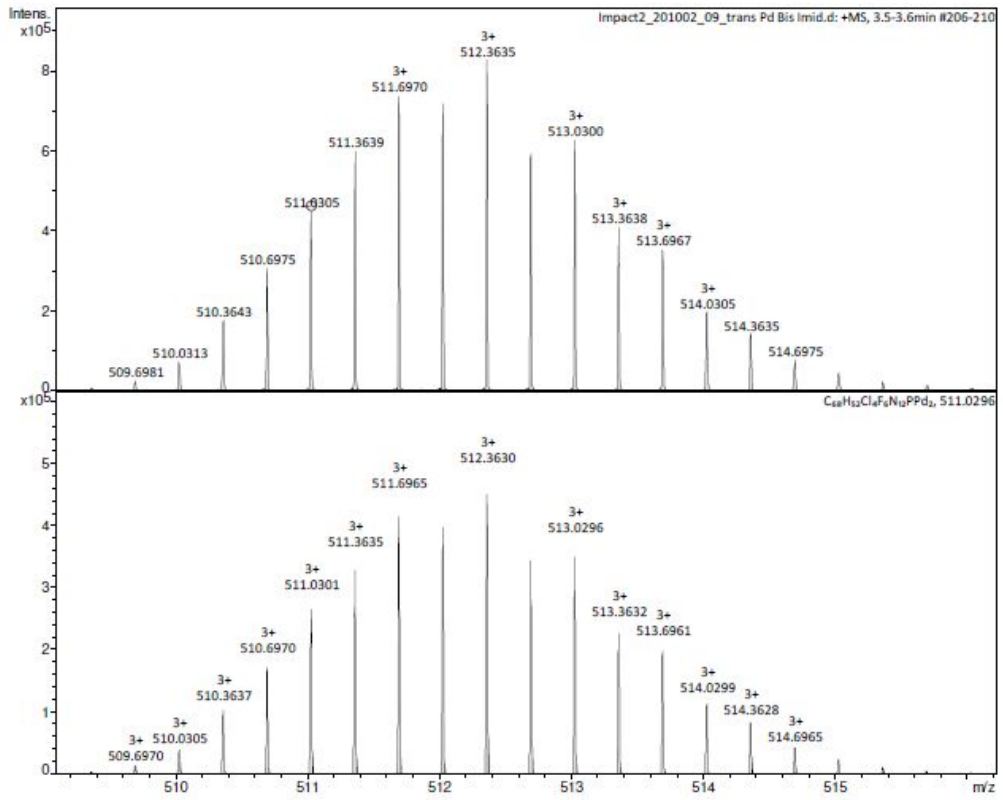

Figure S3. HRMS spectrum of $[(PdCl_2)_2(\mathbf{1}^{2+})_2(PF_6^-)]^{3+}$ (ESI+, z=3+)
Calc (down) for $C_{68}H_{52}Cl_4F_6N_{12}PPd_2$: 511.0296, found (up) 511.0335

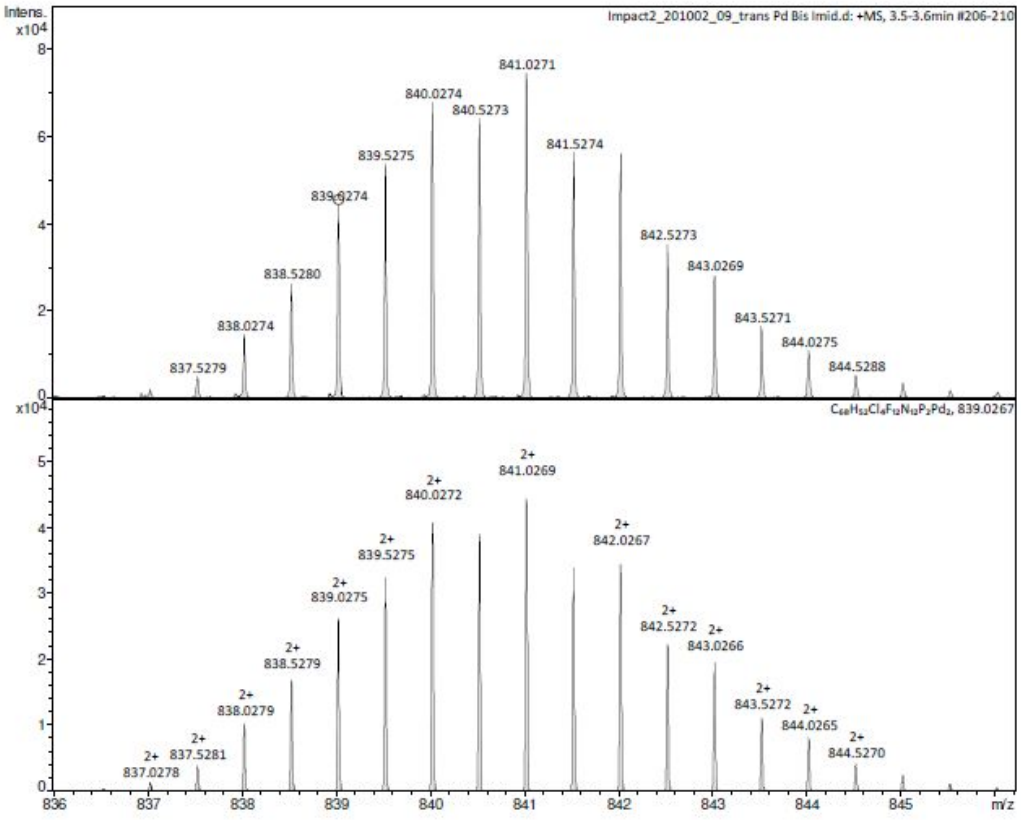

Figure S4. HRMS spectrum of $[(PdCl_2)_2(\mathbf{1}^{2+})_2(PF_6^-)_2]^{2+}$ (ESI+, z = 2+).
Calc (down) for $C_{68}H_{52}Cl_4F_{12}N_{12}P_2Pd_2$: 839.0267, found (up) 839.0274

4. ^{1}H- and ^{13}C-NMR spectra

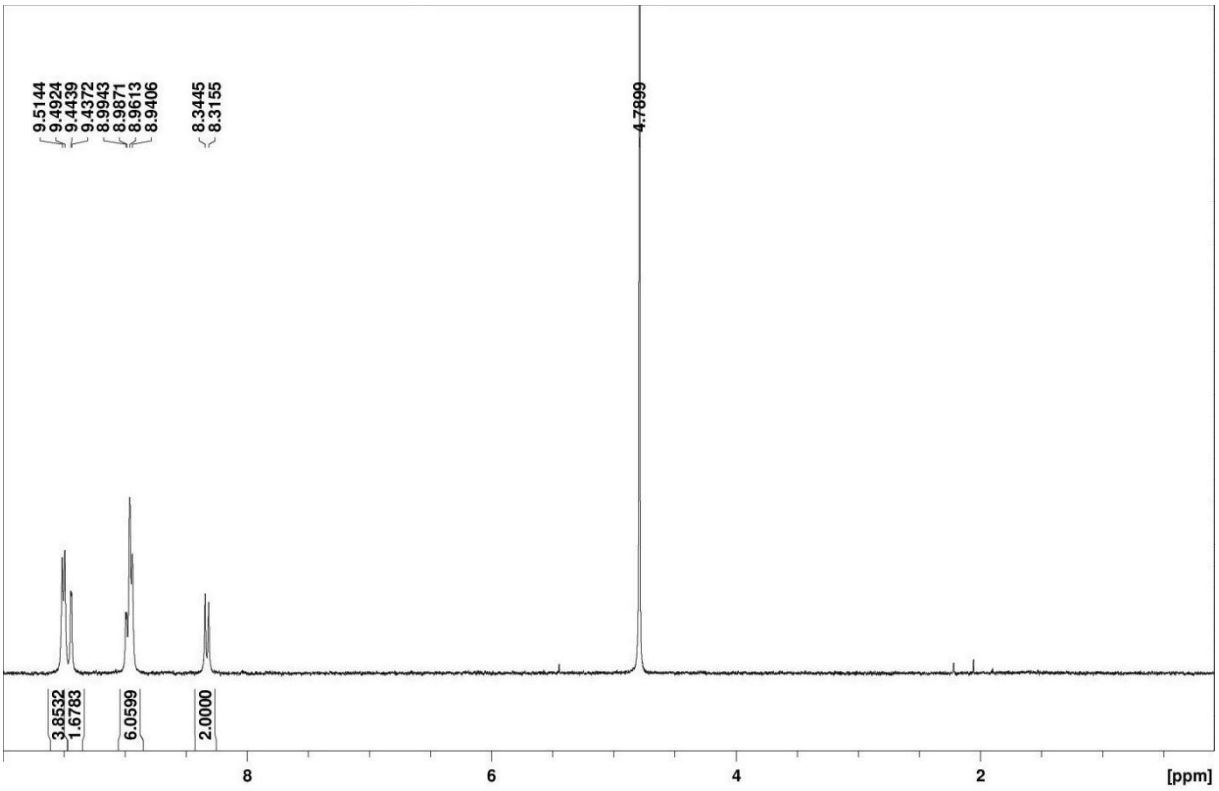

Figure S5. ^{1}H-NMR spectrum of $\mathbf{2}^{2+}$ (300 MHz, D_2O)

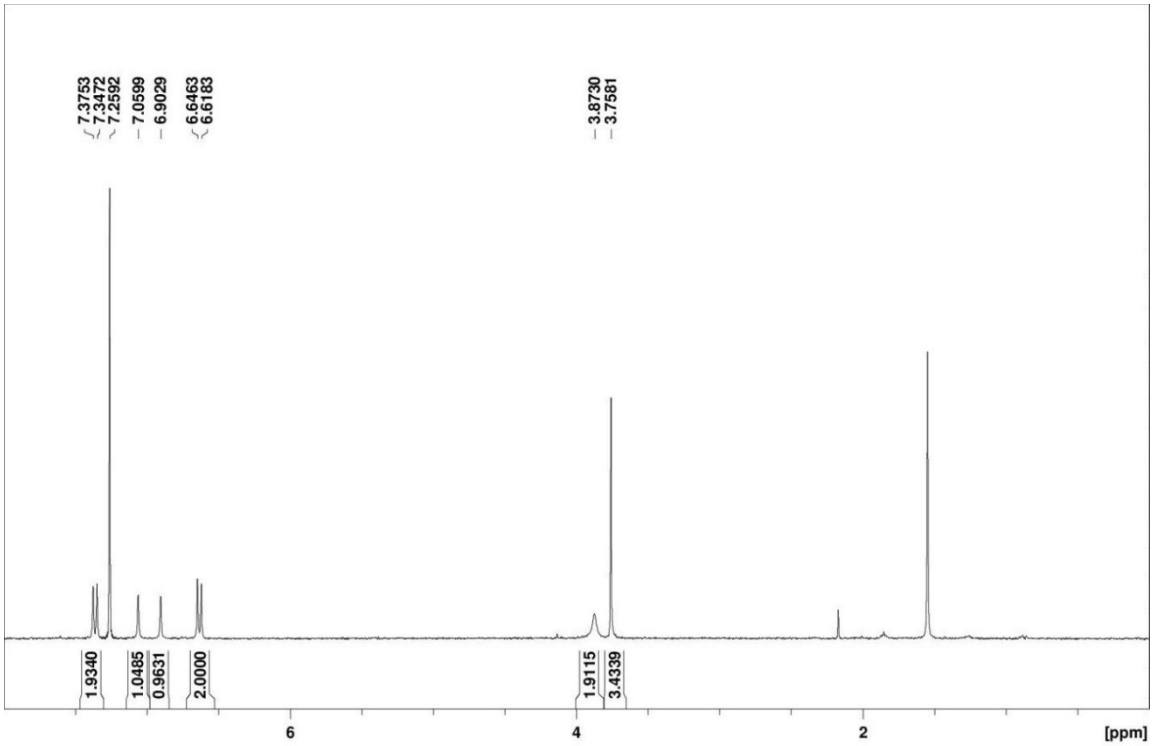

Figure S6. ^{1}H-NMR spectrum of **3** (300 MHz, $CDCl_3$)

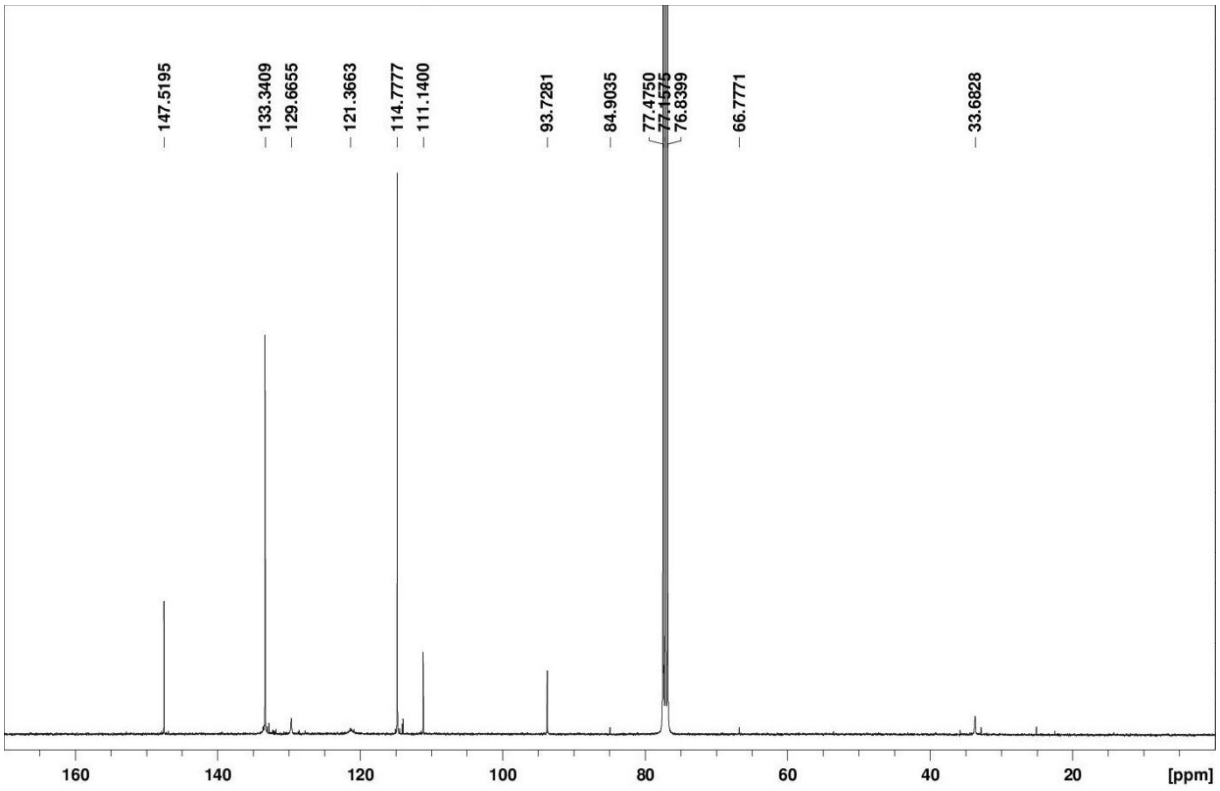

Figure S7. ^{13}C-NMR spectrum of **3** (100 MHz, $CDCl_3$)

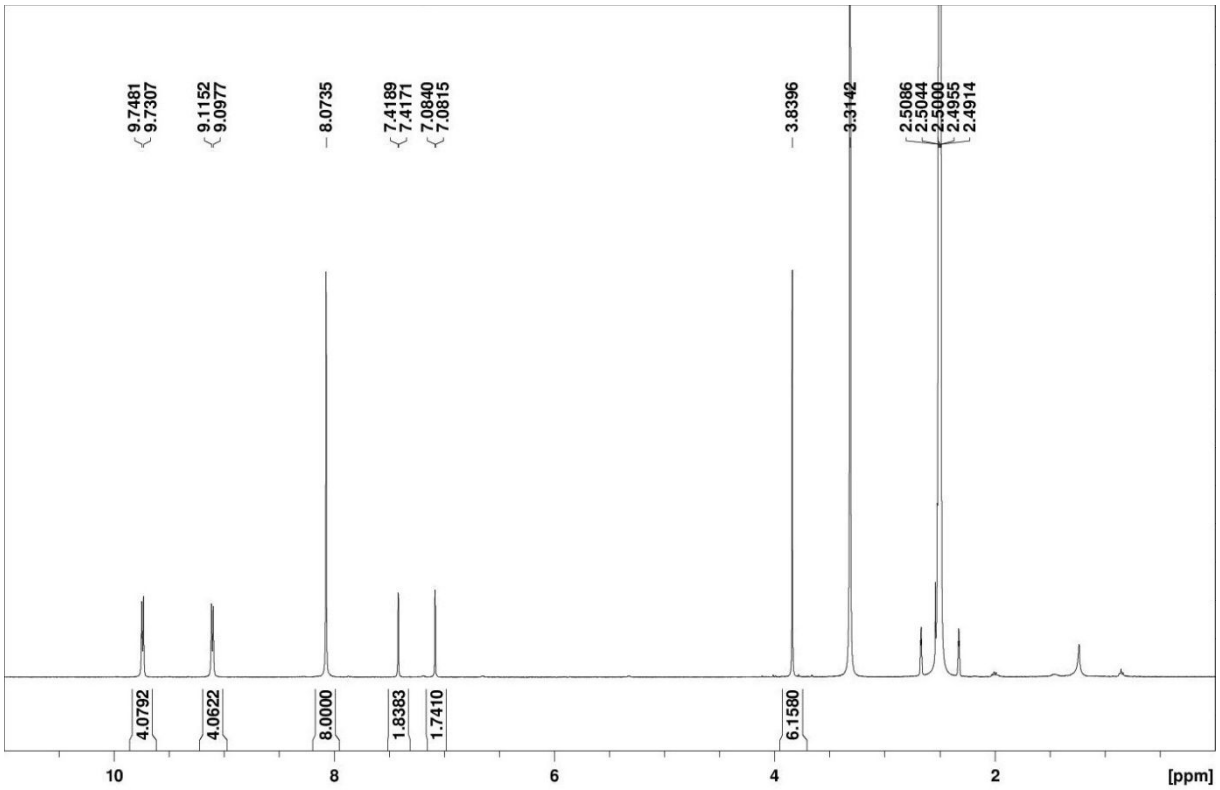

Figure S8. ^{1}H NMR spectra of **1**$(PF_6)_2$ (400 MHz, DMSO-d_6)

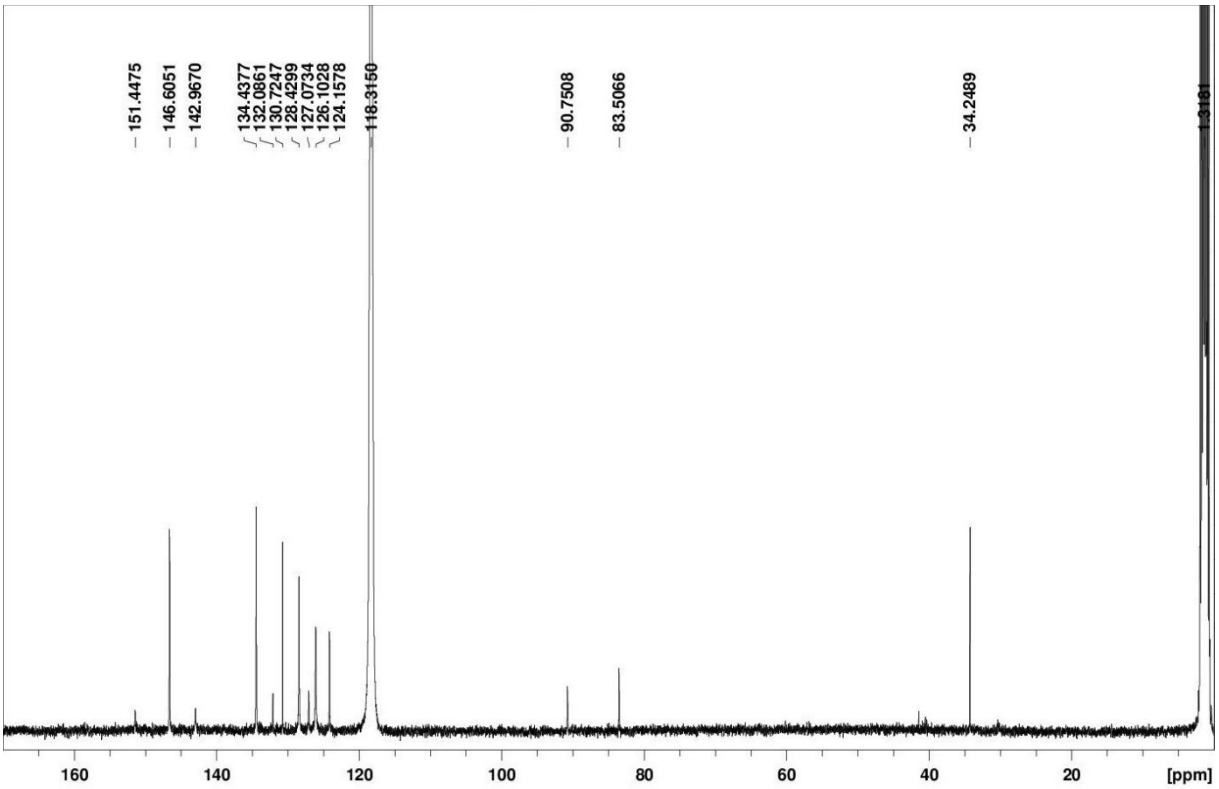

Figure S9. ^{13}C-NMR of **1**$(PF_6)_2$ (100 MHz, CD_3CN).

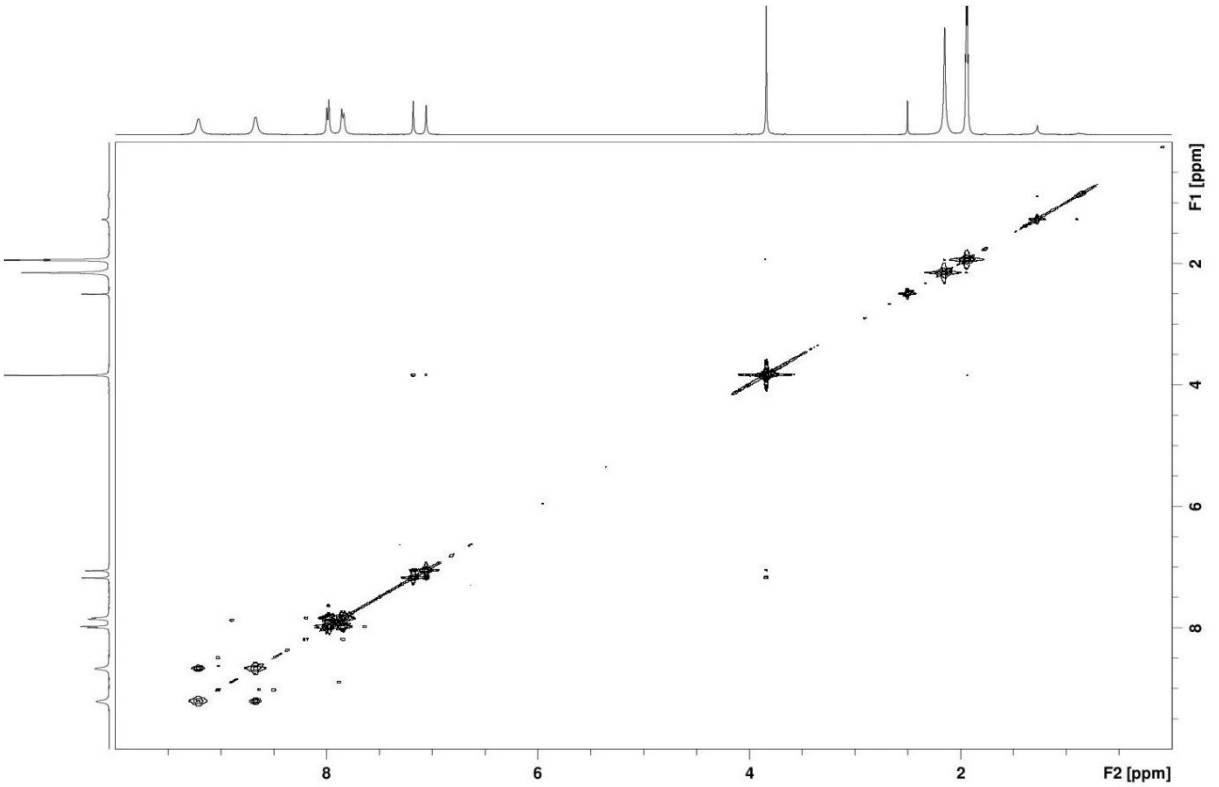

Figure S10. COSY map of **1**$(PF_6)_2$ (400 MHz, CD_3CN)

5. Complexation with palladium

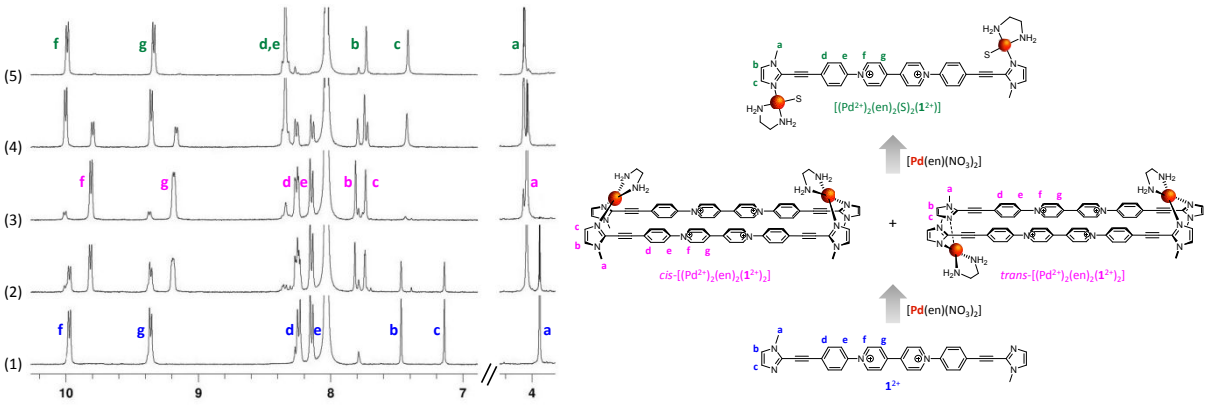

Figure S11. Partial ^{1}H NMR spectra (400 MHz, DMF-d_7, 1.0 mM, 293 K) of **1**$(PF_6)_2$ (1) in the absence, and in the presence of (2) 0.5 equiv. of $[Pd(en)(NO_3)_2]$, (3) 1.0 equiv. of $[Pd(en)(NO_3)_2]$, (4) 10 equiv. of $[Pd(en)(NO_3)_2]$, (5) 200 equiv. of $[Pd(en)(NO_3)_2]$.

6. Electrochemical measurements

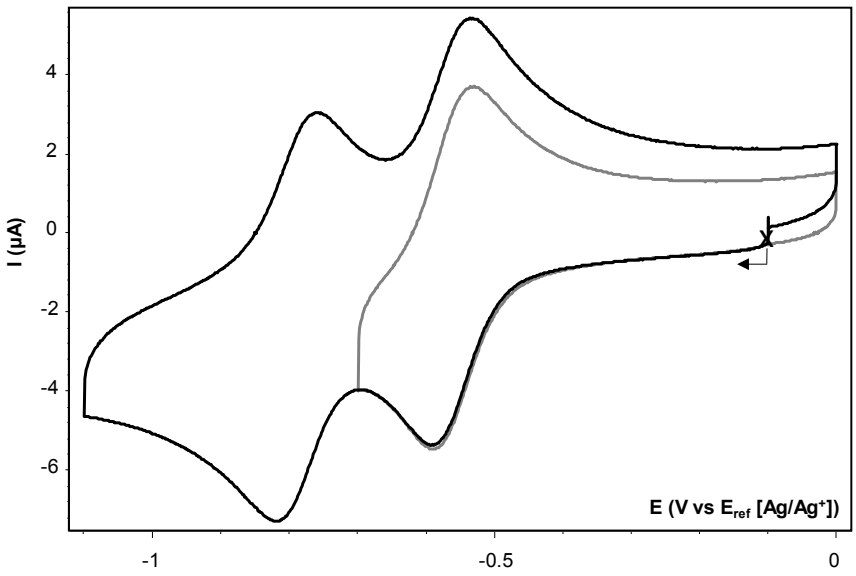

Figure S12. Voltammogram recorded for **1**$(PF_6)_2$ (0.4 mM, DMF+TBAP 0.1 M) (VC, Ø = 3 mm, *E* vs Ag/Ag^+ 10^{-2} M, *v* = 0.1 V s^{-1}).

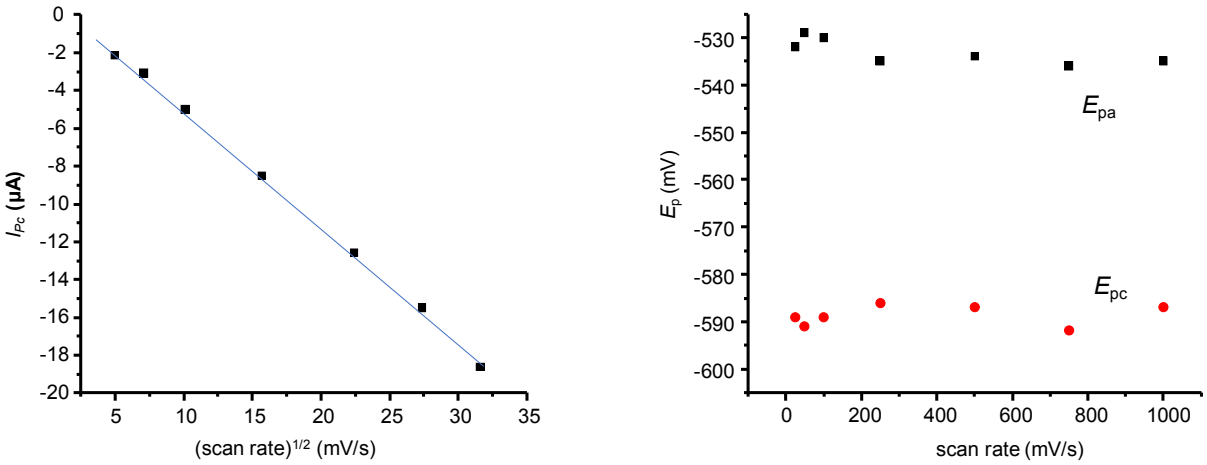

Figure S13. Peak current and peak potential values recorded for **1**$(PF_6)_2$ (0.4 mM, DMF+TBAP 0.1 M) by cyclic voltametry (VC, Ø = 3 mm, *E* vs Ag/Ag^+ 10^{-2} M, *v* = 0.1 V s^{-1}).

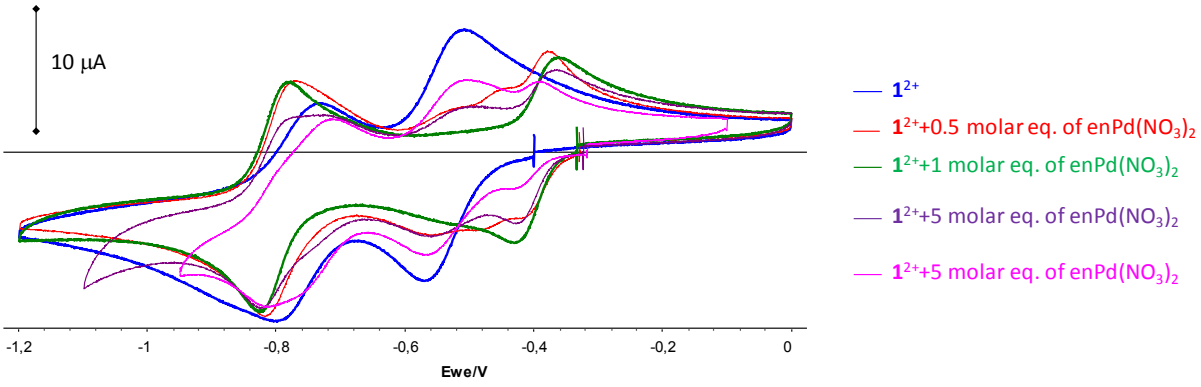

Figure S14. Voltammograms recorded for **1**$(PF_6)_2$ (0.4 mM, DMF+TBAP 0.1 M) in the presence of *cis*-$[Pd(NO_3)_2(en)]$ (VC, Ø = 3 mm, *E* vs Ag/Ag^+ 10^{-2} M, *v* = 0.1 V s^{-1}).

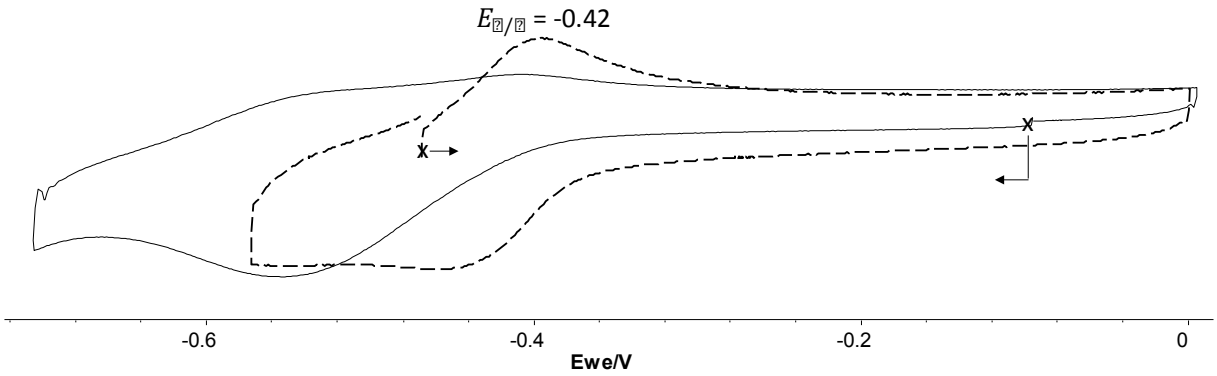

Figure S15. Voltammetric curve (dashed line) measured after exhaustive electrochemical reduction (E_{app} = -0.67 V, one electron/viologens) of a 1:1 (M:L) mixture of **1**$(PF_6)_2$ and $[Pd(ACN)_4](PF_6)_2$ (0.4 mM, DMF+TBAP 0.1 M, vitreous carbon WE, Ø = 3 mm, *E* vs Ag/Ag^+ 10^{-2} M, *v* = 0.1 V s^{-1}). A curve recorded before electrochemical reduction is shown in full line for comparison (1 mM, DMF+TBAP 0.1 M, vitreous carbon WE, Ø = 3 mm, *E* vs Ag/Ag^+ 10^{-2} M, *v* = 0.1 V s^{-1}; normalized current scales).

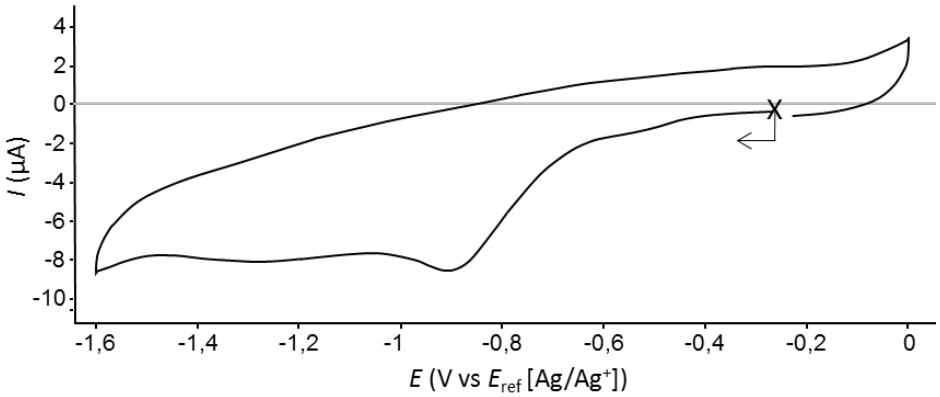

Figure S16. Voltammetric curves measured for *trans*-$[Pd(Cl)_2(CH_3CN)_2]$ in DMF + TBAP 0.1 M (arbitrary concentration, VC, Ø = 3 mm, E vs Ag/Ag+ 10^{-2} M, v = 0.1 V s^{-1})

7. Computational methods

Optimized geometries for the three supramolecular boxes were built manually using Molden, and optimized using density functional theory using the M06-2X[S6] density functional, with the double-zeta Pople's basis set 6-31G(d)[S7] and the use of the Lanl2DZ pseudo-potential for the palladium atoms. All DFT calculations were performed with the Gaussian16 Rev. B.01[S8] suite of programs, and solvation in N,N-dimethylformamide was taken into account through the IEF-PCM (polarization continuum model) model with default parameters.

The geometries for the stationary points corroborate an interaction between the two central viologen arms, whose orientation is dependent on the substitution on the palladium center. Such an interaction is absent in the oxidized states, as the boxes adopt an ellipsoidal shape with a distance between the center of the viologen moieties ranging between 9.2 and 11.7 Å. The structures illustrate the molecular "breathing" of the structures upon two-electron reduction. For the dimer with chlorine ligand in *cis* conformation, the geometry optimization of the oxidized dimer from the p-stacked structure spontaneously led to the separation of the two viologen moeities. For the two other systems, there is presumably an energetic barrier and we perform a relaxed scan to guide the system towards a more stable, "balloon"-like conformation.

It is also noteworthy that a direct energetic comparison between the *cis* and *trans* isomers of $[(\mathrm{PdCl_2})_2(\mathbf{1}^+)_2]^{2+}_{\mathrm{Dim}}$ can be proposed, as shown in Figure ESI 15, and help to situate the impact of the structural distortion on the coupling strength of the viologen units.

The energetic deviation between the viologen moieties and the corresponding reference systems (π-stacked viologens, 56 atoms) was estimated by extracting the Cartesian coordinates of the boxes and adding capping methyl. The energetic diagram given in Figure ESI 15 corroborates a less favorable interaction between the viologen moieties for the $trans$-$[(\mathrm{PdCl_2})_2(\mathbf{1}^+)_2]^{2+}_{\mathrm{Dim}}$. The latter can also be visualized by plotting the HOMO of the three systems, which show a lower overlap for the *trans* conformer (Figure ESI 16).

TDDFT calculations at the ωB97X-D/6-311+G(d,p) level of theory were performed on cis-$[(\mathrm{Pd(en)_2})_2(\mathbf{1}^+)_2]^{6+}_{\mathrm{Dim}}$ to corroborate a transition at 993 nm (f=0.09), followed by two other transitions at 653 and 441 nm. The neat agreement with the measured spectra corroborates the structures provided by the computational approach.

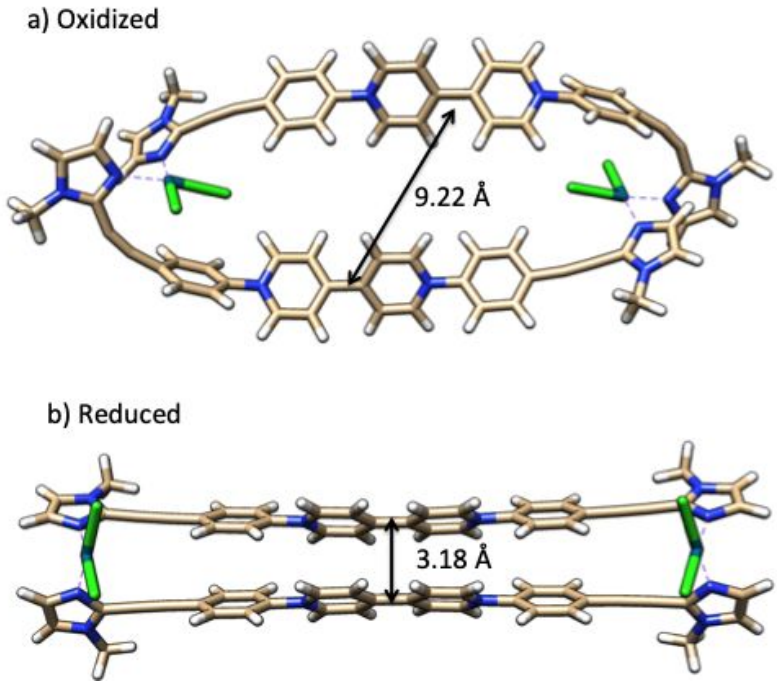

Figure S17. Structures of *cis*-$[(PdCl_2)_2(\mathbf{1}^{+})_2]^{2+}_{Dim}$ and *cis*-$[(PdCl_2)_2(\mathbf{1}^{2+})_2]^{2+}_{Dim}$ after DFT optimization.

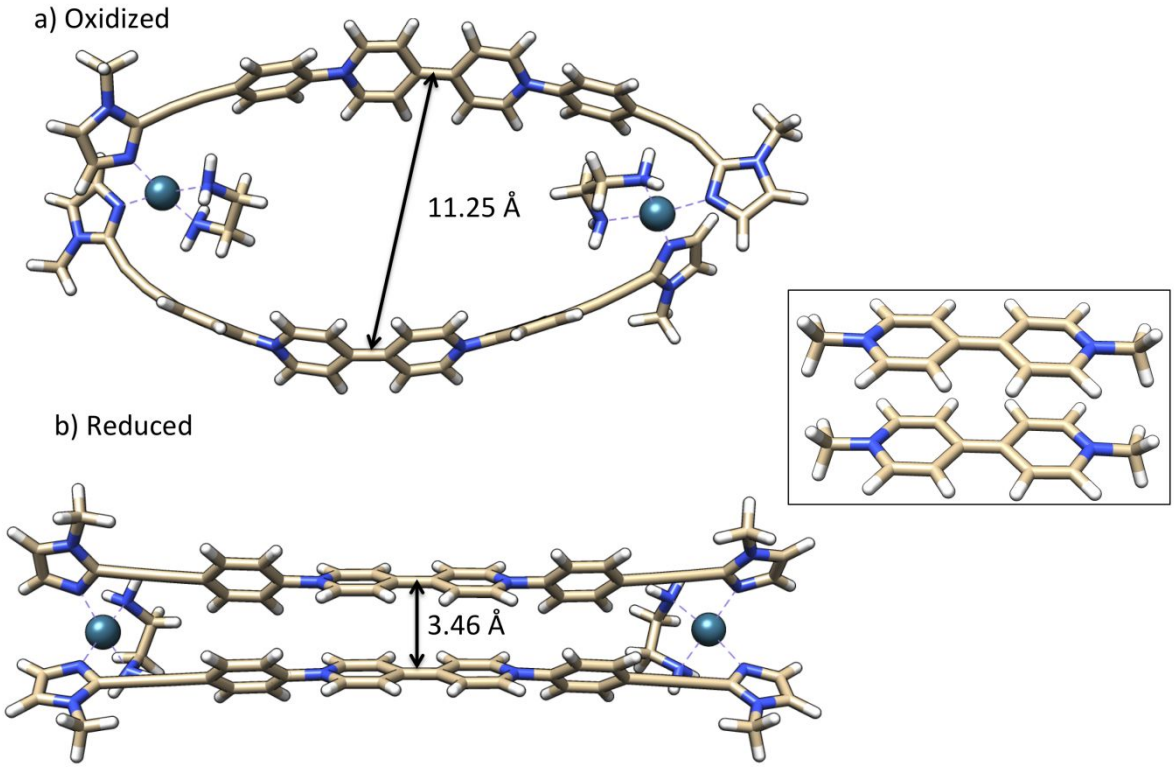

Figure S18. Structures of *cis*-$[(Pd(en))_2(\mathbf{1}^{2+})_2]^{8+}$ and *cis*-$[(Pd(en)_2)_2(\mathbf{1}^{+})_2]^{6+}_{Dim}$ after DFT optimization.

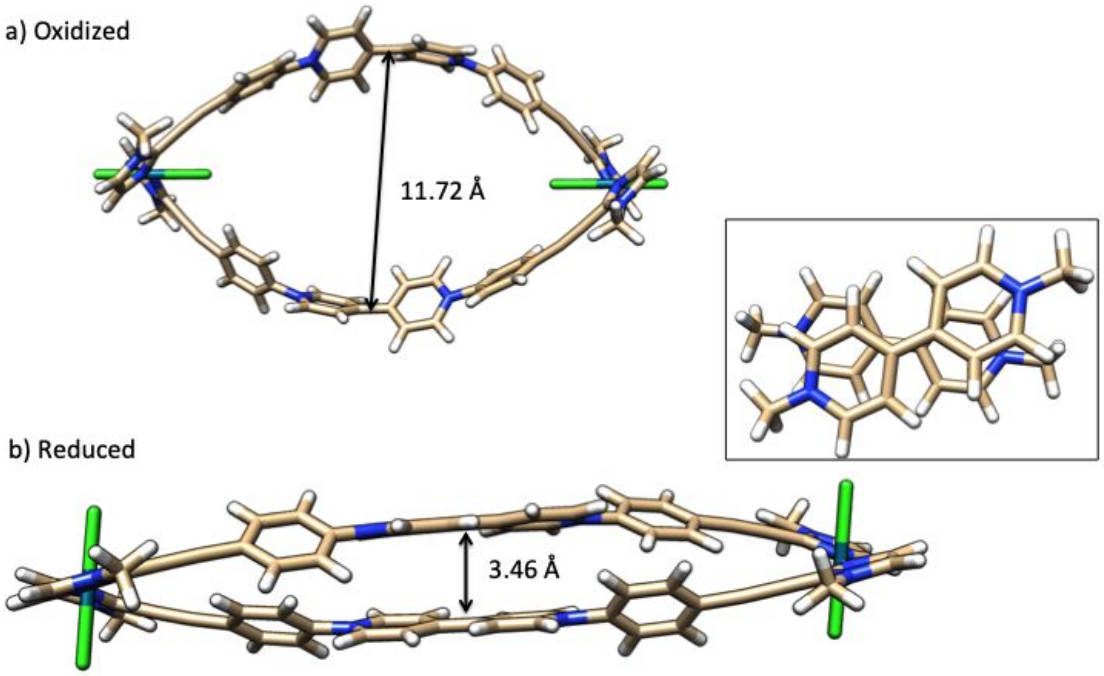

Figure S19. Structures of $trans$-$[(\mathrm{PdCl_2})_2(\mathbf{1}^{+})_2]^{2+}_{\mathrm{Dim}}$ and $trans$-$[(\mathrm{PdCl_2})_2(\mathbf{1}^{2+})_2]^{2+}_{\mathrm{Dim}}$ after DFT optimization. The inset magnifies the twist induced on the viologen central moieties for this isomer.

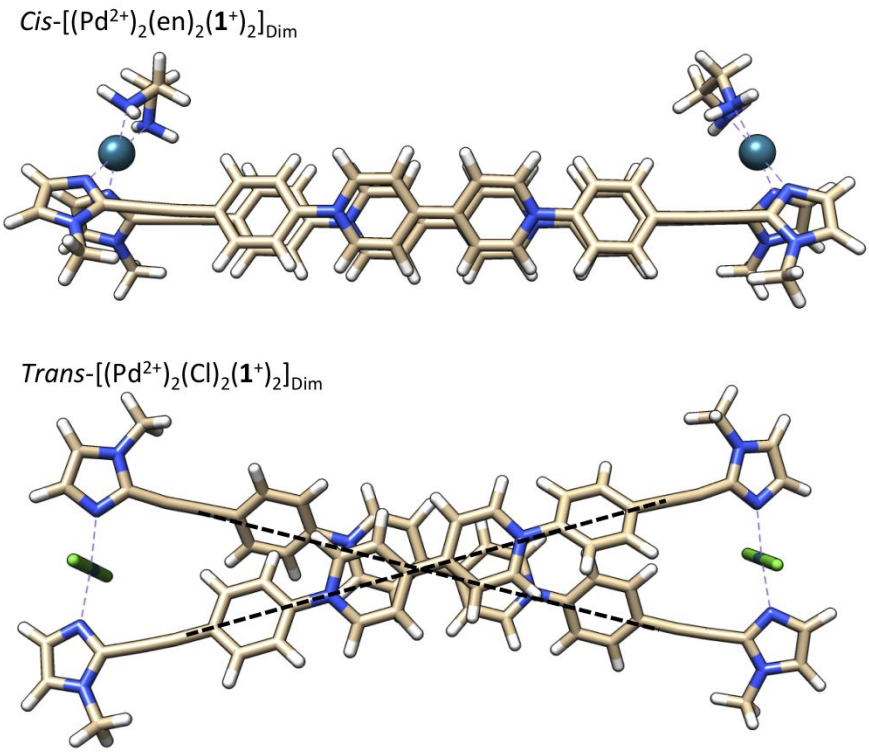

Figure S20. DFT optimized structures for the pi-dimers formed upon reduction of the viologen units *cis*-$[Pd(en)_2(NO_3)_2]$ and *trans*-$[Pd(Cl)_2(CH_3CN)_2]$

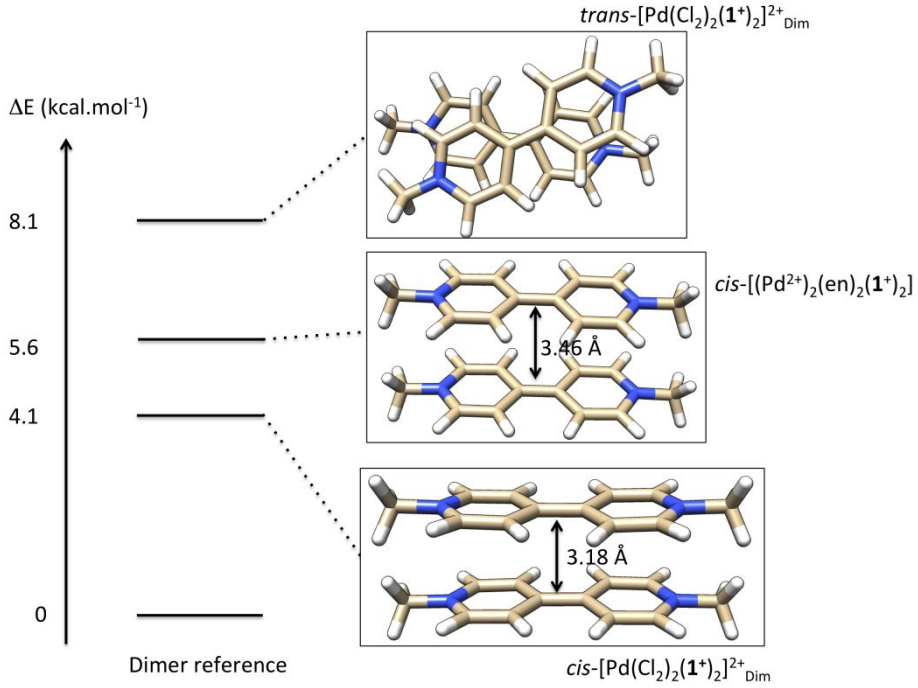

Figure S21. Relative energies of the viologen dimer in its geometries in the three boxes, reflecting the structural deviation from the "ideal", not constrained π-stacked dimer.

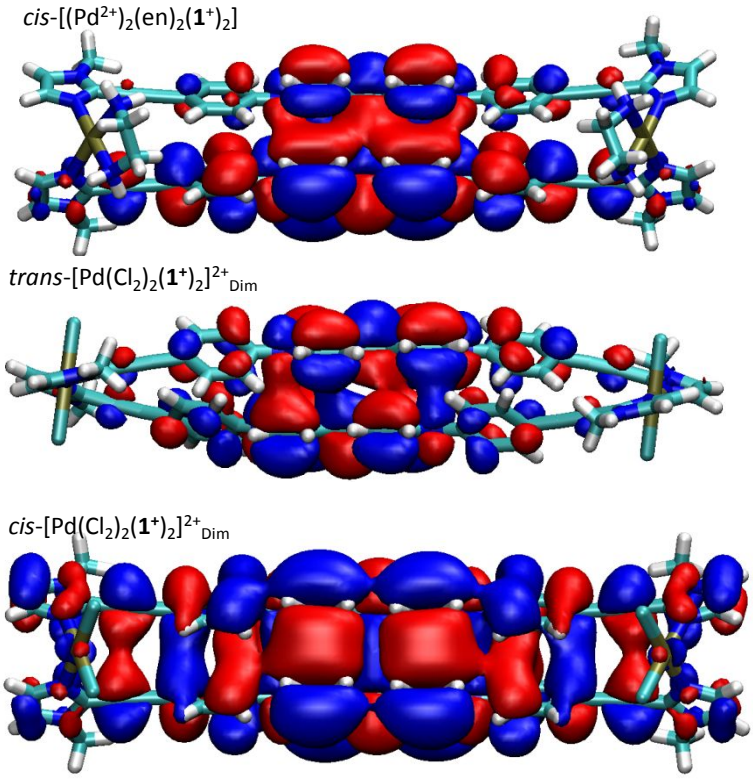

Figure S22. Highest occupied molecular orbital (HOMO) for the reduced dimers, obtained after DFT geometry optimizations (see text for the level of theory). The isovalues of positive and negative phases are 0.03 and −0.03 a.u., respectively. The *trans* isomer singles out by a lower orbital overlap.

Vertical transitions for the three reduced dimers were computed using the time-dependent density functional theory (TDDFT), using the Gaussian 16 Rev B.01 series of programs. Calculations were started from the optimized geometries obtained at the M06-2X/6-31G(d) level of theory. For the excited state calculations, the CAM-B3LYP-D3BJ functional was used, together with the 6-311+G(d,p) basis set.

We note that the intensities are, as always in TDDFT, less accurate than the estimation of the maximum absorption wavelengths. The agreement with experimentally recorded spectra is satisfactory, and our calculations allow to identify at ~800 nm a weak transition (f=0.04) for a HOMO -> LUMO transition that lies higher in energy due to the twisted spatial arrangement of the viologen moieties. The peak is shifted toward higher absorption wavelengths (986 and 940 nm respectively) as cis-conformers are considered.

	cis-$[(Pd^{2+})_2(en)_2(\mathbf{1}^+)_2]$		*cis*-$[Pd(Cl_2)_2(\mathbf{1}^+)_2]^{2+}{}_{Dim}$		*trans*-$[Pd(Cl_2)_2(\mathbf{1}^+)_2]^{2+}{}_{Dim}$
Transitions	*Simulated* λ(nm), f(a.u.)	*Exp.* λ(nm), ε ($L.mol^{-1}.cm^{-1}$)	*Simulated* *λ(nm), f(a.u.)*	*Exp.* λ(nm), ε ($L.mol^{-1}.cm^{-1}$)	*Simulated* *λ(nm), f(a.u).*
1	986.8 (0.13)	1033 (4900)	940.2 (0.12)	1000 (4500)	802.3 (0.04)
2	650.3 (0.48)	656 (35200)	652.4 (0.77)	651 (29100)	640.4 (0.34)
3	614.0 (1.56)	619 (30800)	597.7 (1.78)	614 (28800)	612.1 (1.56)
4	471.2 (5.47)	460 (47200)	467.2 (2.47)	457 (46400)	444.4 (0.47)

Table S1. Properties of the four most significant first transitions (in terms of intensity) computed by TD-DFT. Oscillator strengths (f) are reported in parenthesis.

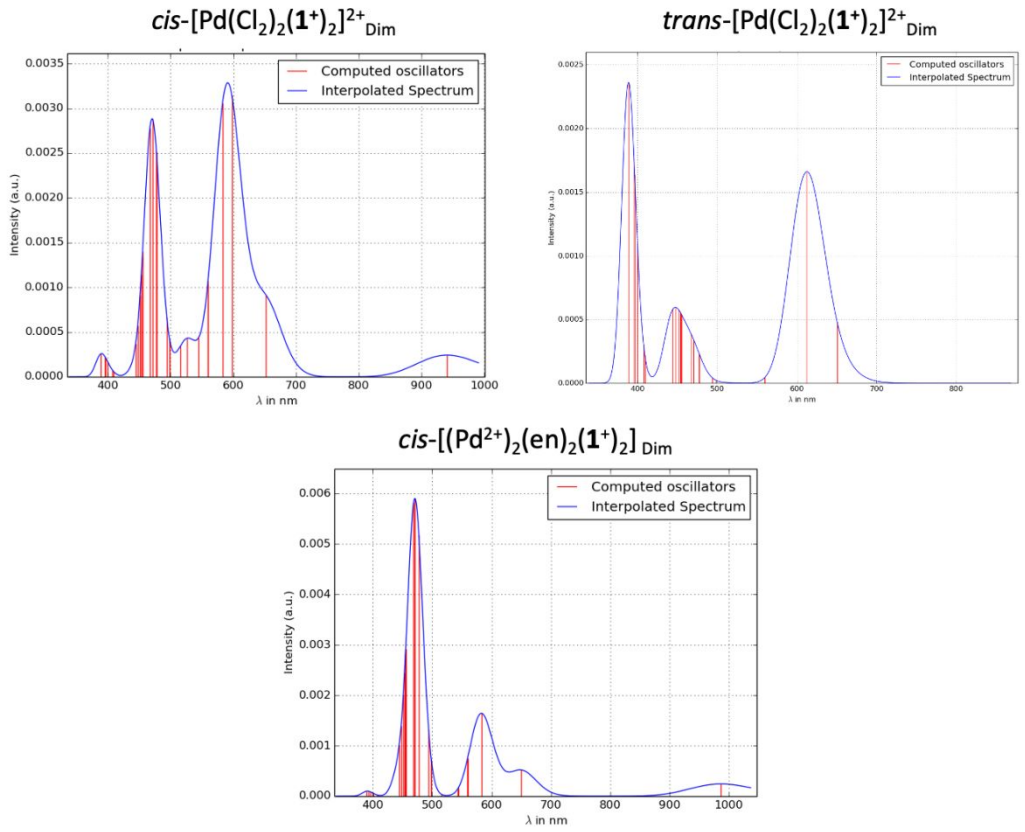

Figure S23. Simulated (blue solid line) absorption spectra for the three reduced dimers, obtained by convoluting TD-DFT stick spectrum (vertical transitions) with Gaussian functions (FWHM=0.2 eV).

8. References

S1 Morell Cerdà, M.; Costisella, B.; Lippert, B. *Inorg. Chim. Acta* **2006**, *359*, 1485-1488

S2 Wimmer, F. L.; Wimmer, S.; Castan, P.; Puddephatt, R. J.. *Inorg. Synth.* **2007**, *29*, 185-187

S3 Kahlfuss, C.; Denis-Quanquin, S.; Calin, N. ; Dumont, E. ; Garavelli, M. ; Royal, G. ; Cobo, S. ; Saint-Aman E. and Bucher, C. *J. Am. Chem. Soc.* 2016, **138**, 15234−15242

S4 Y. Song, X. Huang, H. Hua, Q. Wang, *Dyes Pigm.* **2017**, *137*, 229-235.

S5 W. He, Y.-C. Ge, C.-H. Tan, *Org. Lett.* **2014**, *16*, 3244-3247.

S6 Y. Zhao, D. G. Truhlar, *Theor. Chem. Acc.* **2008**, *120*, 215-241.

S7 V. A. Rassolov, J. A. Pople, M. A. Ratner, T. L. Windus, *J. Chem. Phys.* **1998**, *109*, 1223-1229.

S8 Gaussian 16, Revision C.01, M. J. Frisch, G. W. Trucks, H. B. Schlegel, G. E. Scuseria, M. A. Robb, J. R. Cheeseman, G. Scalmani, V. Barone, G. A. Petersson, H. Nakatsuji, X. Li, M. Caricato, A. V. Marenich, J. Bloino, B. G. Janesko, R. Gomperts, B. Mennucci, H. P. Hratchian, J. V. Ortiz, A. F. Izmaylov, J. L. Sonnenberg, D. Williams-Young, F. Ding, F. Lipparini, F. Egidi, J. Goings, B. Peng, A. Petrone, T. Henderson, D. Ranasinghe, V. G. Zakrzewski, J. Gao, N. Rega, G. Zheng, W. Liang, M. Hada, M. Ehara, K. Toyota, R. Fukuda, J. Hasegawa, M. Ishida, T. Nakajima, Y. Honda, O. Kitao, H. Nakai, T. Vreven, K. Throssell, J. A. Montgomery, Jr., J. E. Peralta, F. Ogliaro, M. J. Bearpark, J. J. Heyd, E. N. Brothers, K. N. Kudin, V. N. Staroverov, T. A. Keith, R. Kobayashi, J. Normand, K. Raghavachari, A. P. Rendell, J. C. Burant, S. S. Iyengar, J. Tomasi, M. Cossi, J. M. Millam, M. Klene, C. Adamo, R. Cammi, J. W. Ochterski, R. L. Martin, K. Morokuma, O. Farkas, J. B. Foresman, and D. J. Fox, Gaussian, Inc., Wallingford CT, 2016.